Modeling and Control of Dynamic Wireless Power Transfer System for Electric Vehicle charger application

Moussa Hassan, Meira Zariff, Karim Kadem, Gilney Damm

Modeling and Control of Dynamic Wireless Power Transfer System for Electric Vehicle charger application

Hassan Moussa*. Zariff Meira*. Karim Kadem*
Gilney Damm**

** Institut VEDECOM, 23 bis Allée des Marronniers, 78000 Versailles, France. (e-mail: hassan.moussa@vedecom.fr) (e-mail: zariff.meira@vedecom.fr), (e-mail: karim.kadem@vedecom.fr)*
*** COSYS-LISIS, Univ. Gustave Eiffel, IFSTTAR, F-77447, Marne-la-Vallée, France. (e-mail: gilney.damm@univ-eiffel.fr)*

Abstract: This paper proposes a nonlinear state-space model for a dynamic wireless power transfer system (DWPT). The DWPT system comprises emitter coils supplied by DC/AC converters, with a phase angle control to achieve maximum power transfer. The power receiver coil is connected to a full bridge diode rectifier followed by an equivalent load resistance. To emulate the dynamic movement property of WPT, the coupling factors between the emitter and receiver coils are set to be variable and depend on the movement of the power receiver alongside the power emitter coils. The control has been successfully demonstrated under variable coupling coefficients to achieve maximum power transfer. Such improvement maintains the power and voltage across the load during transient states.

Keywords: Dynamic wireless charging, electric vehicle battery charger, inductive power transfer, coupling factor, modeling, control design

1. INTRODUCTION

Nowadays, Electric Vehicles (EVs) have been introduced as an alternative method of transportation due to their several advantages such as mitigating environmental issues, carbon emissions and fuel consumption, as well as their remarkable efficiency and being less noisy vehicles. These EVs have battery packs that can be charged by onboard battery chargers [1, 2, 3] which are set to be the conventional wired charging technology commercially available. Recently, the development of wireless charging systems for electric vehicles (EVs) has slowly picked up momentum, mostly over the past decade [4, 5, 6, 7, 8, 9]. With wireless charging systems properly integrated into vehicles and situated strategically around a city, as well as at owners' homes, there is the promise of never needing to plug in an EV again. The basic principle behind the technology is electromagnetic induction. In particular, the use of resonant inductive coupling which involves adding a capacitor to each induction coil to create two resonant circuits (LC circuits) with a specific resonance frequency.

The wireless charging system consists of a boost power factor correction (PFC) converter, DC-AC resonant inverter, and the primary and secondary coils followed by a DC-DC converter for charging the battery. A typical WPT charging system scheme for EVs is reported in Fig. 1.

The transfer of power is done from one magnetic coil in the charging pad to another one fitted to the car. Both coils can be centimeters apart and need to be aligned to obtain the maximum coupling factor. In wireless power transfer, the leakage inductance of the transformer is much larger than the magnetizing inductance due to the large airgap between the primary and secondary coils. To compensate this large leakage inductance, series capacitors are connected to both coils to become a resonant network. The DC/AC inverter supplying the primary coil needs to operate at a switching frequency equal to the resonant frequency of the LC network. Thus, the operating frequency is an input variable that need to be adjusted to control the power transfer.

Modeling and dynamic analysis of the overall system is necessary for designing a closed-loop control for these converters. The most used modeling technique for pulse width modulated (PWM) converters is the state-space averaging approach. This method converts the AC state variables to DC values with slow dynamics by using a synchronous *dq* reference frame transformation [10, 11, 12]. This approach has been shown to be useful for modeling resonant converters under large signal variation and controller design [13].

The purpose of this paper is to utilize the state-space averaging method in DWPT equivalent circuit to design a phase shift control loop for resonant converters by achieving a maximum power delivery and autonomously tracking the resonance frequency ensuring a soft switching of power electronic components. The rest of the paper is focused on the dynamic charging by emulating the car movement by changing the coupling coefficient between secondary and primary coils. The paper highlights the basic control design and simulation using MATLAB.

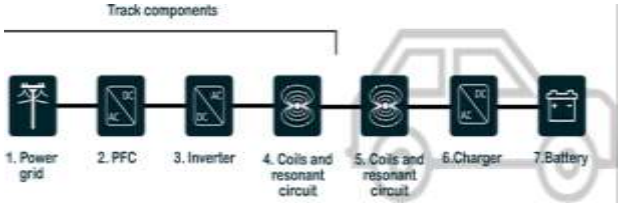

Fig. 1. Typical WPT charging system for EVs.

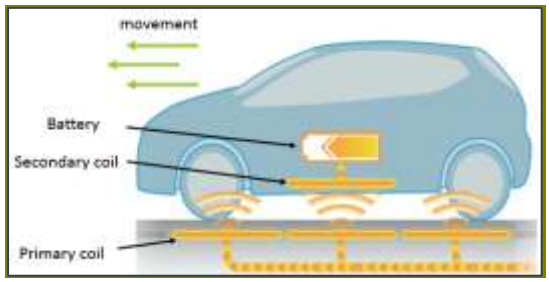

Fig. 2. Dynamic induction charging of an electric vehicle.

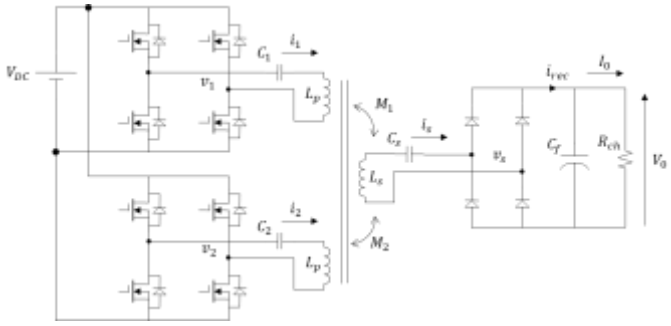

Fig. 3. Equivalent circuit of DWPT system.

2. Dynamic Wireless Power Transfer System

2.1 General Description

The DWPT explored in this study relies on the equivalent circuit that represent the resonant converter with magnetic resonant coupling between the primary ground coil and the secondary vehicle coil as shown in Fig. 2.

The system is free of communication between the primary and secondary side. Due to the large airgap between the primary and secondary coils, the leakage inductance of the transformer is large. To compensate this large inductance, capacitors are added to both sides of the transformer. A series-series compensation is mostly used since its design is independent of the mutual inductance and load. The system suffers from power variation when the coupling factors, system parameters and load change. To address these issues, the model of DWPT system operating at different parameters is considered in the next part.

2.2 Studied DWPT System

The circuit diagram representing the series-series DWPT system is shown in Fig. 3. The dual active bridge (DAB) converter in the primary side converts the DC voltage (V_{DC}) into a full square wave voltage at a switching frequency (ω_s) equal to the resonant frequency of the LC network. The converter at the secondary side is a rectifier that converts the secondary AC voltage (v_s) to an output DC voltage (V_0) after adding an output filter capacitor (C_f) followed by a resistive load R_{ch}. For simplicity and due to the repeating sequence, the DWPT system is considered having two primary windings as the transition from one to another is similar all the way during the vehicle movement on the charging track. The studied system is designed for a rated power of 30 kW. The primary and secondary coils are assumed to be identical so that their self-inductance is the same ($L_p = L_s = L$). In order to simplify the model, the analysis is carried out at the fundamental frequency of the resonant network (ω_s) and the output voltage of the converters are considered as perfect sine wave, v_1 and v_2, which are represented as:

$$v_1 = \frac{4V_{DC}}{\pi} \cdot \sin(\omega_s t) \tag{1}$$

$$v_2 = \frac{4V_{DC}}{\pi} \cdot \sin(\omega_s t) \tag{2}$$

3 Average State-Space Model

In this section, a nonlinear state-space model is derived at fundamental resonant frequency, then all the periodic variables are represented by a Fourier series terms to derive what we called *dq* model. These *dq* terms represent the magnitudes of the sine and cosine of each electric variable.

3.1 Nonlinear state space model

Applying Kirchhoff Voltage Law (KVL) to the circuit of Fig. 3 and deriving the induced voltage due to the mutual impedance, one obtains:

$$v_1 = v_{C1} + r_1 i_1 + L\frac{di_1}{dt} - M_1\frac{di_s}{dt} \tag{3}$$

$$v_2 = v_{C2} + r_2 i_2 + L\frac{di_2}{dt} - M_2\frac{di_s}{dt} \tag{4}$$

$$v_s = -v_{Cs} - r_s i_s - L\frac{di_s}{dt} + M_1\frac{di_1}{dt} + M_2\frac{di_2}{dt} \tag{5}$$

Where, i_1 and i_2 represent the output current of converter 1 and 2 respectively, while i_s is the secondary rectifier input current, and r_1, r_2 and r_s are the primary and secondary resistances.

M_1 and M_2 represent the mutual inductance between each primary and secondary winding, and are represented as (k_1 and k_2 are the coupling coefficients):

$$M_1 = k_1 L \tag{6}$$

$$M_2 = k_2 L \tag{7}$$

Equation (3)-(5) are rearranged and solved to get the following expressions:

$$\frac{di_1}{dt} = \frac{1}{\xi}\left[\frac{-r_1}{\sigma_1 L} i_1 - \frac{r_1}{\sigma_1\sigma_2 L} k_1 i_s - \frac{r_1}{\sigma_1\sigma_2 L} k_1 k_2 i_2 - \frac{k_1}{\sigma_1\sigma_2 L}(v_s + v_{Cs}) + \frac{1}{\sigma_1 L}(v_1 - v_{C1}) + \frac{k_1 k_2}{\sigma_1\sigma_2 L}(v_2 - v_{C2})\right] \tag{8}$$

$$\frac{di_2}{dt} = \frac{1}{\xi}\left[\frac{-r_2}{\sigma_2 L} i_2 - \frac{r_2}{\sigma_1\sigma_2 L} k_2 i_s - \frac{r_2}{\sigma_1\sigma_2 L} k_1 k_2 i_1 - \frac{k_2}{\sigma_1\sigma_2 L}(v_s + v_{Cs}) + \frac{1}{\sigma_1 L}(v_2 - v_{C2}) + \frac{k_1 k_2}{\sigma_1\sigma_2 L}(v_1 - v_{C1})\right] \quad (9)$$

$$\frac{di_s}{dt} = \frac{1}{\xi}\left[\frac{-r_1}{\sigma_1\sigma_2 L} k_1 i_1 - \frac{r_2}{\sigma_1\sigma_2 L} k_2 i_2 - \frac{r_s}{\sigma_1\sigma_2 L} i_s - \frac{1}{\sigma_1\sigma_2 L}(v_s + v_{Cs}) + \frac{k_1}{\sigma_1\sigma_2 L}(v_1 - v_{C1}) + \frac{k_2}{\sigma_1\sigma_2 L}(v_2 - v_{C2})\right] \quad (10)$$

Given, $\sigma_1 = 1 - k_1^2$, $\sigma_2 = 1 - k_2^2$ and $\xi = 1 - \frac{(k_1 k_2)^2}{\sigma_1\sigma_2}$.

The remaining state variables, the series capacitor voltages v_{C1}, v_{C2}, v_{Cs} and the output voltage V_0 of the complete system are described by (11-14).

$$\frac{dv_{C1}}{dt} = \frac{1}{C_1} i_1 \quad (11)$$

$$\frac{dv_{C2}}{dt} = \frac{1}{C_2} i_2 \quad (12)$$

$$\frac{dv_{Cs}}{dt} = \frac{1}{C_s} i_s \quad (13)$$

$$\frac{dV_0}{dt} = \frac{1}{C_f}[i_{rec} - I_0] \quad (14)$$

Where, $i_{rec} = |i_s| = \frac{2}{\pi} i_{s,peak}$ is the rectifier output current and $I_0 = \frac{V_0}{R_{ch}}$, the load current.

Equations (8-14) represent the exact nonlinear state-space model of DWPT system represented by Fig. 3.

3.2 Model in dq synchronous frame

All the state variables are periodic and can be represented by a Fourier series. The power transfer mainly occurs at the fundamental frequency of the resonant network and therefore, modeling is done at the fundamental frequency ω_s. Each AC state variable is represented by its own sine and cosine terms described by the following equation.

$$x_i = x_{id}\sin(\omega_s t) + x_{iq}\cos(\omega_s t) \quad (15)$$

The amplitudes x_{id} and x_{iq} represent the new system state variables replacing the AC terms of the nonlinear model. Substituting (15) on each AC state variable of the model represented in (8-14), a new *dq* model is obtained as:

$$\frac{di_{1d}}{dt} = \frac{1}{\xi}\left[\frac{-r_1}{\sigma_1 L} i_{1d} - \frac{r_1}{\sigma_1\sigma_2 L} k_1 i_{sd} - \frac{r_1}{\sigma_1\sigma_2 L} k_1 k_2 i_{2d} - \frac{k_1}{\sigma_1\sigma_2 L}(v_{sd} + v_{Csd}) + \frac{1}{\sigma_1 L}(v_{1d} - v_{C1d}) + \frac{k_1 k_2}{\sigma_1\sigma_2 L}(v_{2d} - v_{C2d})\right] + \omega_s i_{1q} \quad (16)$$

$$\frac{di_{1q}}{dt} = \frac{1}{\xi}\left[\frac{-r_1}{\sigma_1 L} i_{1q} - \frac{r_1}{\sigma_1\sigma_2 L} k_1 i_{sq} - \frac{r_1}{\sigma_1\sigma_2 L} k_1 k_2 i_{2q} - \frac{k_1}{\sigma_1\sigma_2 L}(v_{sq} + v_{Csq}) + \frac{1}{\sigma_1 L}(v_{1q} - v_{C1q}) + \frac{k_1 k_2}{\sigma_1\sigma_2 L}(v_{2q} - v_{C2q})\right] - \omega_s i_{1d} \quad (17)$$

$$\frac{di_{2d}}{dt} = \frac{1}{\xi}\left[\frac{-r_2}{\sigma_2 L} i_{2d} - \frac{r_2}{\sigma_1\sigma_2 L} k_2 i_{sd} - \frac{r_2}{\sigma_1\sigma_2 L} k_1 k_2 i_{1d} - \frac{k_2}{\sigma_1\sigma_2 L}(v_{sd} + v_{Csd}) + \frac{1}{\sigma_1 L}(v_{2d} - v_{C2d}) + \frac{k_1 k_2}{\sigma_1\sigma_2 L}(v_{1d} - v_{C1d})\right] + \omega_s i_{2q} \quad (18)$$

$$\frac{di_{2q}}{dt} = \frac{1}{\xi}\left[\frac{-r_2}{\sigma_2 L} i_{2q} - \frac{r_2}{\sigma_1\sigma_2 L} k_2 i_{sq} - \frac{r_2}{\sigma_1\sigma_2 L} k_1 k_2 i_{1q} - \frac{k_2}{\sigma_1\sigma_2 L}(v_{sq} + v_{Csq}) + \frac{1}{\sigma_1 L}(v_{2q} - v_{C2q}) + \frac{k_1 k_2}{\sigma_1\sigma_2 L}(v_{1q} - v_{C1q})\right] - \omega_s i_{2d} \quad (19)$$

$$\frac{di_{sd}}{dt} = \frac{1}{\xi}\left[\frac{-r_1}{\sigma_1\sigma_2 L} k_1 i_{1d} - \frac{r_2}{\sigma_1\sigma_2 L} k_2 i_{2d} - \frac{r_s}{\sigma_1\sigma_2 L} i_{sd} - \frac{1}{\sigma_1\sigma_2 L}(v_{sd} + v_{Csd}) + \frac{k_1}{\sigma_1\sigma_2 L}(v_{1d} - v_{C1d}) + \frac{k_2}{\sigma_1\sigma_2 L}(v_{2d} - v_{C2d})\right] + \omega_s i_{sq} \quad (20)$$

$$\frac{di_{sq}}{dt} = \frac{1}{\xi}\left[\frac{-r_1}{\sigma_1\sigma_2 L} k_1 i_{1q} - \frac{r_2}{\sigma_1\sigma_2 L} k_2 i_{2q} - \frac{r_s}{\sigma_1\sigma_2 L} i_{sq} - \frac{1}{\sigma_1\sigma_2 L}(v_{sq} + v_{Csq}) + \frac{k_1}{\sigma_1\sigma_2 L}(v_{1q} - v_{C1q}) + \frac{k_2}{\sigma_1\sigma_2 L}(v_{2q} - v_{C2q})\right] - \omega_s i_{sd} \quad (21)$$

$$\frac{dv_{C1d}}{dt} = \frac{1}{C_1} i_{1d} + \omega_s v_{C1q} \quad (22)$$

$$\frac{dv_{C1q}}{dt} = \frac{1}{C_1} i_{1q} - \omega_s v_{C1d} \quad (23)$$

$$\frac{dv_{C2d}}{dt} = \frac{1}{C_2} i_{2d} + \omega_s v_{C2q} \quad (24)$$

$$\frac{dv_{C2q}}{dt} = \frac{1}{C_2} i_{2q} - \omega_s v_{C2d} \quad (25)$$

$$\frac{dv_{Csd}}{dt} = \frac{1}{C_s} i_{sd} + \omega_s v_{Csq} \quad (26)$$

$$\frac{dv_{Csq}}{dt} = \frac{1}{C_s} i_{sq} - \omega_s v_{Csd} \quad (27)$$

$$\frac{dV_0}{dt} = \frac{1}{C_f}\left[\frac{2}{\pi} i_{s,peak} - \frac{V_0}{R_{ch}}\right] \quad (28)$$

Where, $i_{s,peak} = \sqrt{i_{sd}^2 + i_{sq}^2}$.

Equations (16)-(28), represent the *dq* model of the nonlinear system of Fig. 3. This model represents the envelope of AC currents and voltages of the resonant network in both steady-state and transient state conditions. The *dq* model can be written in the form:

$$\frac{d}{dt}x = f(x,u) \qquad y = g(x,u) \quad (29)$$

Where,

$$x = [i_{1d}\ i_{1q}\ i_{2d}\ i_{2q}\ i_{sd}\ i_{sq}\ v_{C1d}\ v_{C1q}\ v_{C2d}\ v_{C2q}\ v_{Csd}\ v_{Csq}\ V_0]^T$$

$$u = [\omega_s\ V_1\ V_2]^T$$

$$y = V_0$$

4 PHASE SHIFT CONTROL DESIGN

The phase shift control algorithm is realized on the emitter side of the DWPT system in order to tune the resonant frequency by tracking the phase shift between the output voltage and current of the converter. The phase shift between the voltage and current is zero at resonant frequency and the power transfer is maximum. Fig. 4 shows the program flow chart of the phase shift control algorithm.

First, the frequency of the converter starts at its maximum value f_0 higher than the resonant frequency. The measured phase angle is compared to a given interval and the controller will determine the optimal correcting value of the switching frequency of the converter. The program executes until the phase shift is at minimum positive value to maintain a Zero Voltage Switching (ZVS) condition of the PWM converter. To ensure ZVS operation, the switching frequency of the converter should be above the resonant frequency. This can be achieved when the output current is lagging the voltage with a slightly minimum phase angle.

To calculate the phase shift from the *dq* model, Fig. 5 describes the phasor diagram of one converter with the assumption that the phase angle of the voltage v_1 is the reference. The phase shift is given as:

$$\delta_1 = \tan^{-1}\left(\frac{i_{1q}}{i_{1d}}\right) \tag{30}$$

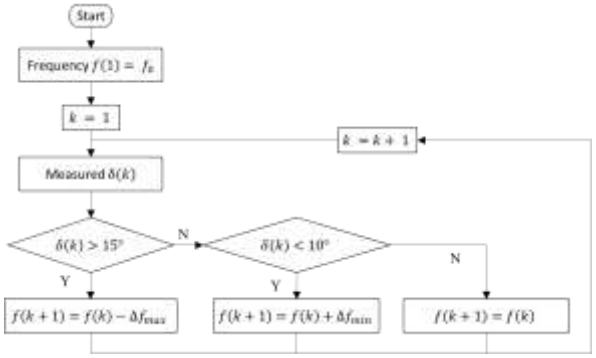

Fig. 4. Flow chart of the phase-shift control algorithm.

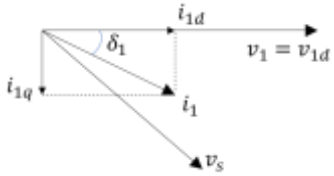

Fig. 5. Phasor diagram of one converter.

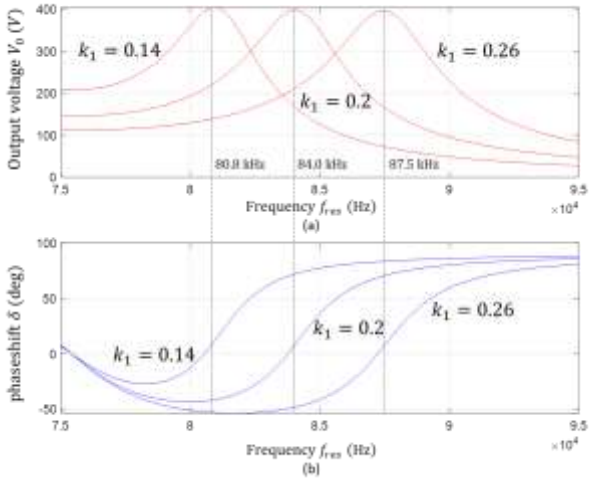

Fig. 6. (a) System output voltage versus switching frequency; (b) phase shift versus switching frequency.

5 Model Validation using Simulation

The model is built on MATLAB with the parameters shown in Table 1. First a simulation is done for one converter suppling a primary coil by varying the coefficient factor k_1 ($k_2 = 0$). Fig. 6 shows the output voltage versus the switching frequency as well as the phase shift for three different coupling coefficients. These steady-state curves give a prediction at which resonant frequency the phase shift control algorithm will settle in order to obtain a maximum power transfer. The maximum output voltage we will obtain is around 400V for a resistive load of $R_L = 5.2\ \Omega$.

Table 1: DWPT system Simulation Parameters

Parameter	Value
Transferred power	30 kW
DC input voltage	450 V
Coupling coefficient	From 0.1 to 0.26
Primary and secondary inductances	$Lp = Ls = L = 135\ \mu H$
Primary and secondary resistance	$r_1 = r_2 = r_s = 0.1\ \Omega$
Load Resistance	$R_L = 5.2\ \Omega$
Output Filter Capacitor	$C_f = 1100\ \mu F$
Primary and secondary resonant capacitor	$33\ nF$
Switching frequency	$80\ to\ 90\ kHz$

In order to test the phase-shift controller a setup simulation is done for $k_1 = 0.26$ and $k_2 = 0$. In this case, one converter is supplying one primary coil with the secondary coil exactly facing the primary coil with 15cm airgap. Fig. 7(a) shows the output *dq* currents passing through the primary winding. The *d*-component is greater than the *q*-component which indicates a minimum phase-shift between the current vector i_1 and the voltage vector v_1 which is aligned to the *d*-axis (i.e., $v_{1d} = 4V_{dc}/\pi$ and $v_{1q} = 0$).

The peak current can be calculated as $i_{1,peak} = \sqrt{i_{1d}^2 + i_{1q}^2} = 122\ A$. Fig. 7(b) shows the *dq* voltages of the series capacitor used to compensate the leakage inductance. The values show a peak voltage equal to 6.72 kV across the capacitor C_1. A high voltage film capacitor is used for this application that can support a voltage of 8500Vrms.

Fig. 8 shows the resonant frequency, the output power and output DC voltage. At steady state, the resonant frequency is equal to 87.67 kHz which is slightly greater than 87.5 kHz (as presented in Fig. 6) since the closed loop phase-shift controller tends to hold a positive value between 10 to 15 degrees. The output power is 29.7 kW with an output voltage of 393.4V as seen in Fig. 8(b) and (c).

The overall system simulation is done by varying the coupling coefficient between the primary coils and the secondary to emulate the dynamic wireless power transfer when the vehicle moves on the charger track. Fig. 9 represents the DWPT system under study showing two converters suppling the primary coils N and N+1. The first converter (N) is set to be on Master state to transfer the power to the load whereas the second converter (N+1) is OFF. Nevertheless, there will be an induced current on the second primary coil, even while the converter is OFF, thanks to the switching ON

of the two lower MOSFETS of the converter. In this way, while the secondary coil (fitted to the car) moves from one primary to another, the magnitude of the currents circulating in the two primary coils change and they are equal when the secondary coil is situated equidistant to the center of the two primary coils. At this moment, the change on switching state occurs. The converter (N+1) is put on Master state, and hence transfer the power to the load, whereas the previous Converter (N) and the next converter (N+2) are set to OFF state by short circuiting their primary coils. The coupling coefficient values are represented on Fig. 10 for two adjacent primary coils with the secondary coil moving alongside them at 15cm airgap. These values are taken by Ansys Maxwell simulator for the primary and secondary coils designed in VEDECOM.

Fig. 11 shows the amplitude of the current circulating through both primary coils. At the beginning, the first converter peak current is maximum while the second converter output current is zero. The current amplitudes are equal when the secondary coil is centered between the two primary coils (i.e., $k_1 = k_2$). The switching state occurs, and the second converter is now supplying the load and its output peak current reaches its maximum value when the secondary coil is aligned to it. Fig. 12(a) shows the resonant frequency of the secondary coil as well as the output power and voltage in Fig. 12(b), (c) when passing from one primary coil to another. Due to the transition from one converter to another the output power decreased to a value defined by the resonant frequency. The output power goes back to its maximum value when passing completely to another coil. The regulation of output voltage at the secondary coil can be designed using a buck-boost DC-DC converter, to maintain an output voltage while charging the battery, which is not in the scope of this article. A constant-current mode operation is usually proposed for such converter to charge an EV battery. Since the input voltage is variable as function of the coupling factor between the primary and secondary coils, a Buck-Boost topology is needed for an EV onboard battery charger.

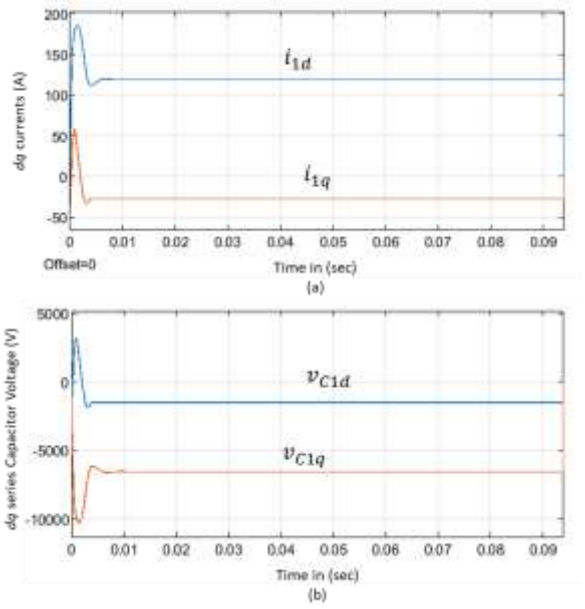

Fig. 7. (a) *dq* output currents of converter 1; (b) *dq* voltage of series capacitor C_1.

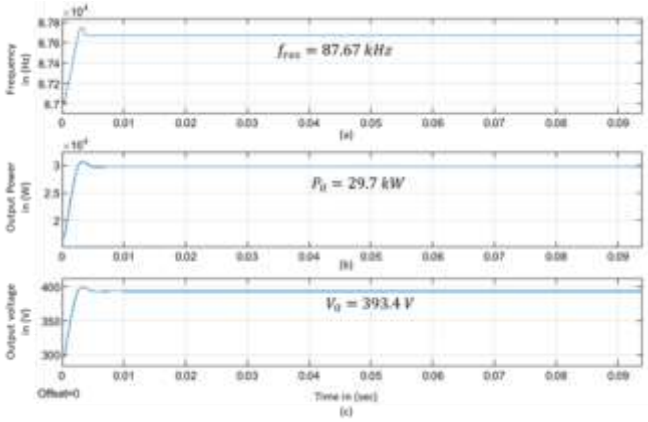

Fig. 8. (a) Resonant frequency; (b) output power; (c) output voltage for the case of one converter supplying a primary coil.

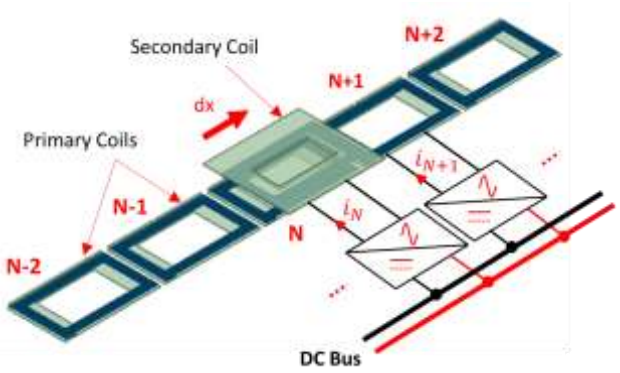

Fig. 9. Primary and secondary coils for the DWPT system.

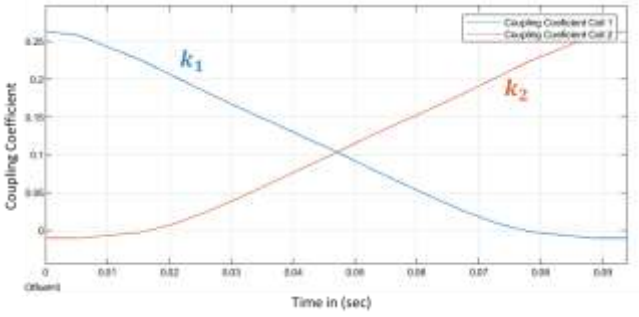

Fig. 10. Coupling coefficients variation as function of the secondary coil movement.

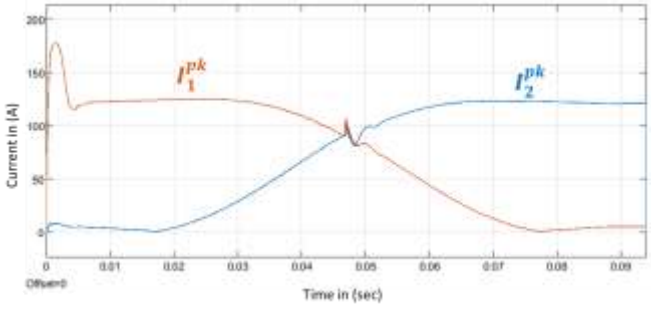

Fig. 11. Peak current circulating through the first and second primary coils.

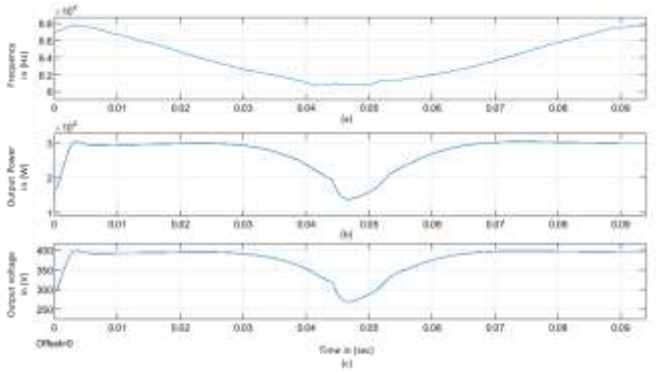

Fig. 12. (a) Resonant Frequency; (b) output power; (c) output voltage of the complete system.

Remark: The proposed algorithm is based on a time varying coupling factor k. The variation of this coupling factor is arbitrary, and it will englobe several variations including the speed of the car (and speed variation), and the mutual impedance coupling from adjacent (N-1 and N+1) coils. Therefore, those effects are being coped with, if the algorithm sample rate is much faster than these variations. What is easy to obtain with even very simple microcontrollers, compared with the speed of real vehicles.

6 Conclusion

This paper has first proposed a nonlinear model of a Dynamic Wireless Power Transfer (DWPT) for EV battery charging applications. An average state-space model is derived by mathematically analyzing the equivalent electric circuit of a DWPT. In the following, a *dq* model of the system is derived by converting all the AC state variables to DC states of slow dynamics which is better suited to simulate and to design the control algorithm. A phase shift hysteresis controller is then proposed for each converter to transfer the maximum power to the secondary side. The objective of this controller is to search the resonant frequency by compensating the phase-shift between the output voltage and current of the converter. A dynamic change of the coupling coefficients is introduced to the model in order to emulate the movement of the car along the charge track. Simulation results show the basic control of power when passing from one primary coil to another by analyzing the magnitude of the output current of the present and following converters. The criteria in comparing the current magnitudes are important since it gives the essential information of the secondary coil position between the primary coils. It was demonstrated that the continuity of power transfer to the load is achieved in this manner.

References

[2] H. Neves de Melo, J. Pedro F. Trovao, P. G. Pereirinha, H. M. Jorge and C. Henggeler Antunes, "A Controllable Biderictional Battery Charger for Electric Vehicles with Vehicle-to-Grid Capability," *IEEE Transactions on Vehicular Technology,* vol. 67, pp. 114-123, 2018.

[3] J. Deng, S. Li, S. Hu, C. C. Mi and R. Ma, "Design Methology of LLC Resonant Converters for Electric Vehicle Battery Chargers," *IEEE Transactions on Vehicular Technology,* vol. 63, pp. 1581-1592, 2014.

[4] D. H. Tran, V. B. Vu and W. Choi, "Design of a High-Efficiency Wireless Power Transfer System with Intermediate Coils for the On-Board Chargers of Electric Vehicles," *IEEE Transactions on Power Electronics,* vol. 33, pp. 175-187, 2018.

[5] H. Wang, U. Pratik, A. Jovicic, N. Hasan and Z. Pantic, "Dynamic Wireless Charging of Medium Power and Speed Electric Vehicles," *IEEE Transactions on Vehicular Technology,* vol. 70, pp. 12552-12566, 2021.

[6] B. Pang, J. Deng, P. Liu and Z. Wang, "Secondary-side power control method for double-side LCC compensation topology in wireless EV charger application," *43rd Annual Conference of the IEEE Industrial Electronics Society (IECON 2017),* 2017.

[7] J.-Y. Lee and B.-M. Han, "A Bidirectional Wireless Power Transfer EV Charger Using Self-Resonant PWM," *IEEE Transactions on Power Electronics,* vol. 30, pp. 1784-1787, 2015.

[8] K. Kadem, Z. Meira, G. Damm and H. Moussa, "Efficient Sequencing Method of ground coils for Dynamic Wireless Power Transfer," *IEEE Wireless Power Week (WPW 2022),* pp. 1-6, 2022.

[9] Z. Meira, G. Damm, K. Kadem and H. Moussa, "A 30 kW Dynamic Wireless Inductive Charging System for EVs," *24th European Conf. on Power Electronics and Applications (EPE'22),* 2022.

[10] A. A. Aboushady, K. H. Ahmed, S. J. Finney and B. W. Williams, "Linearized Large Signal Modeling, Analysis, and Control Design of Phase-Controlled Series-Parallel Resonant Converters Using State Feedback," *IEEE Transactions on Power Electronics,* vol. 28, pp. 3896-3911, 2013.

[11] W. Louis Malan, D. M. Vilathgamuwa and G. R. Walker, "Modeling and Control of a Resonant Dual Active Bridge with a Tuned CLLC Network," *IEEE Transactions on Power Electronics,* vol. 31, 2016.

[12] P. Chi-Kwong Luk, S. Aldhaher, W. Fei et J. F. Whidborne, "State-Space Modeling of a Class E2 Converter for Inductive Links," *IEEE Transactions on Power Electronics,* vol. 30, pp. 3242-3251, 2015.

[13] Z. U. Zahid, Z. M. Dalala, C. Zheng, R. Chen, W. Eric Faraci, J.-S. Jason Lai, G. Lisi and D. Anderson, "Modeling and Control of Series–Series Compensated Inductive Power Transfer System," *IEEE Journal of Emerging and Selected Topics in Power Electronics,* vol. 3, pp. 111-123, 2015.

G. Bin, L. Chien-Yu, C. Baifeng, J. Dominic and L. Jih-Sheng, "Zero-Voltage-Switching PWM Resonant Full-Bridge Converter with Manimized Circulting Losses and Minimal Voltage Stresses of Bridge Rectifiers for Electric Vehicle Battery Chargers," *IEEE Transactions on Power Electronics,* vol. 28, pp. 1132-1144, 2013.